

## REAL: 1.5 MICRON WAVELENGTH SCANNING POLARIZATION LIDAR

Shane D. Mayor, Scott M. Spuler, Bruce M. Morley, Eric Loew,  
Tammy M. Weckwerth, Stephan De Wekker, and Daniel J. Kirshbaum

National Center for Atmospheric Research  
Earth Observing Laboratory  
P.O. Box 3000, Boulder, Colorado, 80307-3000, USA

### ABSTRACT

Since the last ILRC, NCAR's Raman-shifted Eye-safe Aerosol Lidar (REAL) has been upgraded to feature backscatter polarization sensitivity and it has been deployed in several field experiments. This paper describes the hardware improvements implemented to enable the polarization capability and observations of various types of aerosol plumes released on a military test range. The REAL was also deployed as part of the NSF sponsored T-REX experiment in March of 2006 in order to visualize the atmospheric flow in the Owens Valley of California. Examples of data from that experiment will be shown. Lastly, we will briefly describe a second generation REAL ("v2") that was created by ITT Industries for continuous and unattended operation.

### 1. MOTIVATION

REAL[1; 2; 3] operates at 1.54 microns wavelength to capitalize on the maximum eye-safety in this wavelength region. The ability to safely transmit high energy pulses allows one to generate strong signal-to-noise ratio (SNR) backscatter from long ranges from a single, or very small number, of pulses. Eye-safety facilitates unattended operation and use of the system in urban areas or near aircraft and airports. The system is intended for use in applications where high-resolution spatial-imagery of the aerosol distribution is desired. Time-lapse animations of the scans can be used to visualize atmospheric motion.

### 2. POLARIZATION CAPABILITY

Depolarization measurements with lidar systems are well known and have been used to identify particle shapes or phases of water in clouds over the past 30 years.[4] For example, it has been demonstrated that spherical particles (i.e. droplets) backscatter linearly polarized laser light in the same polarization plane.[5; 6] As a particle's shape deviates from spherical, some of the incident light is backscattered in other polarization planes. For example, crystals are highly depolarizing. Therefore, by examining the depolarization of a condensed water cloud,



Figure 1. The Raman-shifted Eye-safe Aerosol Lidar (REAL "v1") resides in a 20-foot shipping container.

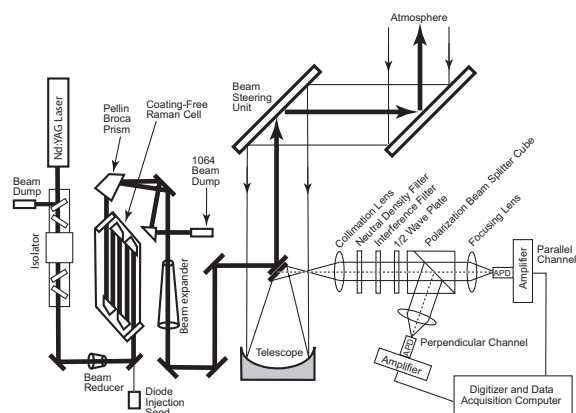


Figure 2. System schematic of the Raman-shifted Eye-safe Aerosol Lidar (REAL) using the coating-free Raman cell and the two-channel depolarization receiver.

one may be able to infer its phase (i.e. liquid or ice). Our intention was to extend this capability to optically thin aerosols. Because REAL is eye-safe and can scan in all directions, this capability should be of use in the stand-off identification and tracking of small aerosol plumes, especially in urban areas.

Obtaining absolute depolarization with a scanning device, like REAL, takes special precautions.[7] Reflection by the scanning mirrors has the effect of rotating the polarization vector of the outgoing laser pulse. Upon propagation back to the receiver, the polarization vector is counter-rotated by the same amount. However, if the aerosols have a preferred orientation, or the mirrors have different reflection coefficients, the absolute measured depolarization will be erroneous. In addition, mirrors impart a small phase difference between the reflected electric field components. This phase difference transforms linear polarization to elliptical which is not restored back to linear by back-propagation. These angle-dependent errors can be minimized with careful attention to the mirror coatings. Currently, protected gold coatings are used on the BSU mirrors. These metallic coatings are inexpensive and considered insensitive to polarization, at least to a first order. The above issue must be addressed to make absolute depolarization measurements.

To implement backscatter depolarization capability on REAL, the polarization purity of the transmit beam was improved by placing an optical isolator at the exit of the Nd:YAG laser. The optical isolator consists of a Faraday rotator and two polarizers (each polarizer is a pair of double dielectric Brewsters plates each with an extinction ratio of  $10^{-4}$ .) This reduces the pump energy entering the Raman cell by about 20 percent to about 615 mJ per pulse. In addition to improving the polarization purity, the isolator protects the pump laser from potential optical feedback. The improved polarization purity is also required for efficient use of the second generation Raman cell which employs six optical elements at the Brewster angle. The polarization purity of the beam transmitted to the atmosphere is well in excess of 10000:1.

The lidar receiver was modified to provide two detection channels: parallel and perpendicular polarization. The first element of the receiver past the telescope is a focusing lens designed to collimate the light for transmission through several subsequent optics. These include a neutral density filter, an interference filter, a 1/2 wave plate, and a calcite air-gap Glan Taylor polarization beam splitter cube. The neutral density filter is part of a filter wheel that allows the backscatter signal to be attenuated to prevent saturation and reduce the risk of damaging the photodetectors from hard target reflections.

The polarization beam splitter cube has a 25 mm clear aperture. Backscattered light returned from the atmosphere in the same polarization plane that was transmitted passes through the cube and is focused on the InGaAs APD on the right side of the diagram (referred to as the parallel channel). The orthogonal polarization state of the backscattered light is reflected out the side of the polar-

ization beam splitter cube at an angle of 109.9 degrees relative to the axis of the parallel beam. This light is focused on to a second InGaAs APD at the center and bottom of the diagram (referred to as the perpendicular channel). The beamsplitter cube has an extinction ratio of  $10^{-6}$  for the transmitted beam. The reflected beam (the perpendicular channel) contains 3% of the parallel polarized light, however it is reflected at a slightly different angle exiting the cube. This difference in angles is sufficiently large given the fast focusing lens and small detector diameter that most (99.7%) of those rays miss the active area. The resulting effective extinction ratio in this channel is  $10^{-4}$ .

Several improvements were made to the detector/amplifier modules as described in Spuler and Mayor.[2] We use Perkin-Elmer C30659-1550-R2A InGaAs APDs. This off-the-shelf component features a photodiode and preamplifier in a single device. The diameter of the active element is 200 microns and the bandwidth of the entire device is 50 MHz. The module provides the ability of adjusting the bias of the photodiode to compensate for changes in temperature. This capability was added for the field tests described in the next section. Photodiode bias stabilization is performed by Labview software that reads a voltage from a temperature-sensing diode contained in the package. The Labview program computes a running 10 s mean of the temperature and adjusts the bias of the detector according to a temperature versus gain function described in the manufacturer's specifications.

The above detector/preamp module is mounted on a custom electronics board with a post amplifier stage in order to (1) provide additional gain, (2) provide adjustability of the voltage offset to fall within the input range of the digitizer, (3) drive a 50 ohm coaxial cable (to allow a large distance between the amplifier and data acquisition computer), and (4) provide adjustable gain so that the equivalent amount of optical power from the two modules have identical signal levels on the data acquisition system. The post amplifier is an AD829 op-amp operating in an inverting configuration.

### 3. FIELD EXPERIENCE AND LIMITATIONS

Our recent field experiences and some lab tests have taught us some important limitations of our above hardware developments. First, the gold coatings on the BSU mirrors do indeed impart an angular dependence to the backscatter depolarization ratio. This systematic error is weak compared to the strong backscatter signal from water clouds. The change of error with respect to scan angle is also sufficiently low that relative changes in depolarization ratio can be detected for even weak optical scattering aerosol features. For example, fig. 3 shows a near-horizontal scan through two aerosol plumes created at Dugway Proving Ground. The left panel shows total scattering intensity and the right panel shows the depolarization ratio. The plume on the left was generated from a

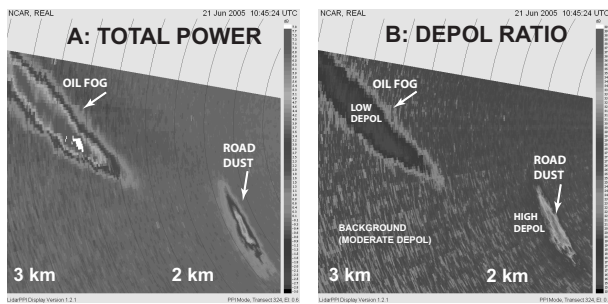


Figure 3. Results of a PPI scan through two different types of aerosol plumes. Left panel (a) total backscatter intensity. Right panel (b) relative depolarization ratio.

point source and is composed of oil droplets. The plume on the right was the result of driving a vehicle on an unpaved road. The relative change in depolarization ratio for these two different types of plumes is significant and consistent with our understanding of the shape of the particles in the plumes.

A second difficulty, discovered recently by laboratory testing, is that the detector/amplifier modules exhibit relevant signal bandwidths on the order of 10 times less than the expected 50 MHz. This is due mostly to the design of the post amplifier stage; in particular the inherent limitations of the AD829 opamp for use in this application. The detector/amplifier signal bandwidth decreases (response time increases) significantly as the gain is increased.

Since two independent detector/amplifier modules are used to measure the depolarization ratio, a slight gain mismatch will result in a mismatch in amplitude response. This leads to inaccuracies in depolarization ratio measurements made near sharp aerosol gradients. The less than expected bandwidth also prevents the system from reaching its maximum possible range resolution.

#### 4. METEOROLOGICAL APPLICATIONS

Despite the limitations as described above, REAL was deployed in several field campaigns during the last two years and we collected some very interesting examples of data. For example, during the June 2005 deployment[3] at Dugway Proving Ground, Utah, we observed the field of coherent structures as show in fig. 4. This near-horizontal sector scan was collected during the evening. The terrain beneath the scan is very flat and covered by brush not exceeding 1 meter tall. The lidar data lie in a quasi-horizontal plane between approximately 10 and 50 meters above the surface. The backscatter image has been high-pass median filtered to remove the large-scale variability and trends such as those caused by extinction. Fig. 4 shows the turbulent coherent structure of the atmospheric surface layer during this time. Information contained in this image includes the spacing, size, shape and orientation of coherent structures.

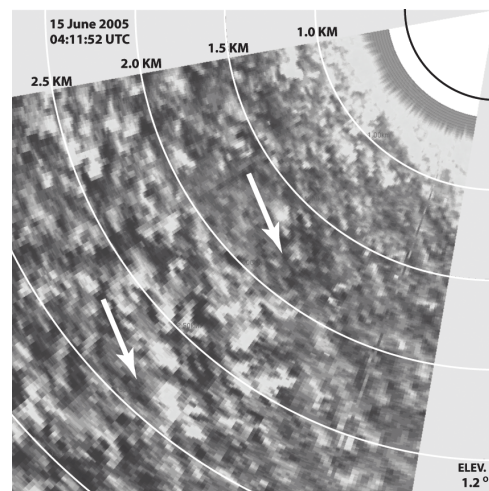


Figure 4. High-pass median filtered PPI scan on 15 June 2005 at Dugway Proving Ground, Utah, shows surface layer coherent structures.

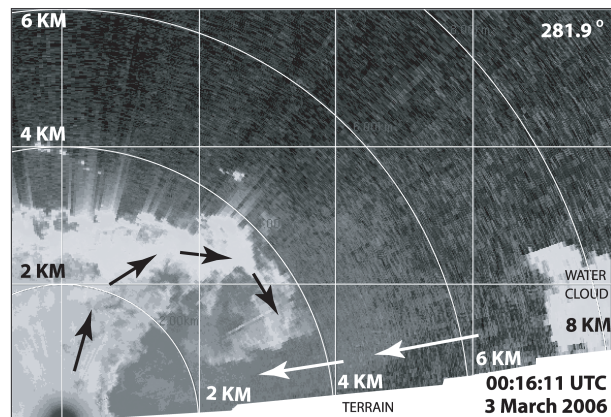


Figure 5. RHI scan from the T-REX field campaign on 3 March 2006 reveals a low aerosol scattering downslope flow while high aerosol scattering air rises and curls over the downslope flow.

REAL was deployed in a large-scale meteorological experiment[8] in March and April 2006 in the Owens Valley, California, to study the effects of mountains on atmospheric flows. For example, strong westerly flows crossing the Sierra mountain range can induce wave and circulation patterns that have important implications for aviation safety and air pollution transport. Fig. 5 shows one frame of an animation of vertical slices which shows the rotation of flow along a horizontal axis. Fig. 6 shows one frame of a sequence that reveals an aerosol layer descending into the Owens Valley. Over the course of time, the position of the wave's trough moves and the steepness of the ascending branch of this wave changes.

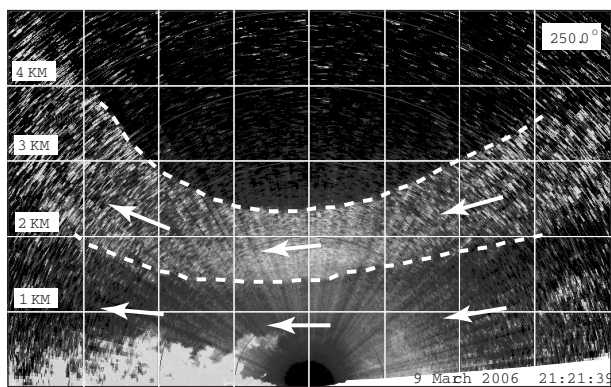


Figure 6. RHI scan from the T-REX field campaign on 9 March 2006 reveals a layer of moderate intensity aerosol scattering between 1.5 and 2.4 km above the lidar site. The layer takes the shape of a large amplitude wave in the flow. Beneath it, dust is lofted from high winds near the surface.

## 5. REAL “V2” AND “V3”

ITT Industries recently completed the design, construction and installation of second generation REAL for unattended and continuous operation. The REAL “v2”, as shown in fig. 7, is contained in a weatherproof enclosure approximately 3 m on each side. The transmitter runs at 20 Hz. A network connection enables remote system monitoring and control.

The next generation REAL (“v3”) currently being developed at NCAR will operate with 350 mJ pulses at 50 Hz for longer range and faster scans. The transmitter improvements are described in a separate paper by Spuler and Mayor in this same conference. We hope to recoat the BSU mirrors with a polarization insensitive coating. We intend to redesign the detector/amplifier to achieve 50 MHz bandwidth over the full dynamic range of the A/D converters employed in the digitizer. In addition, we plan to characterize the noise in the present detector/amplifier and to optimize the SNR in the future design.

## ACKNOWLEDGMENTS

Many individuals in the Earth Observing Laboratory at NCAR have contributed to REAL and its field deployments. We are especially indebted to the Design and Fabrication Services staff. NCAR is sponsored by the U.S. National Science Foundation (NSF).

## REFERENCES

1. Mayor, S. D. and Spuler, S. M. Raman-shifted eye-safe aerosol lidar (real). *Appl. Optics*, 43:3915–3924, 2004.

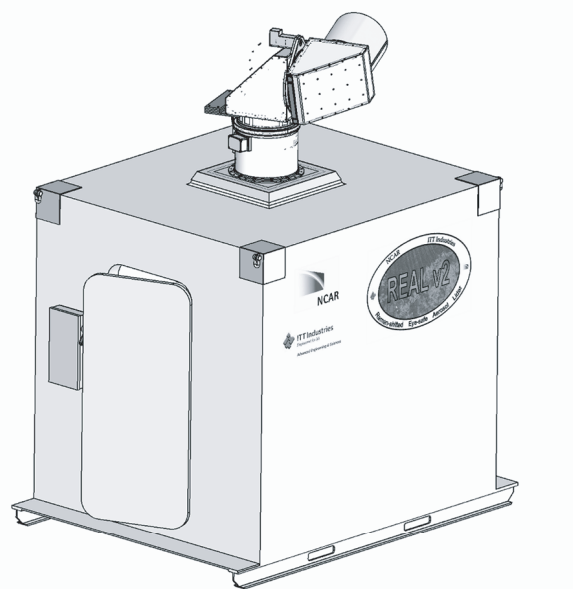


Figure 7. The first REAL “v2” was created by ITT Industries in November of 2005 for continuous and unattended operation. It has been in operation since then for an aerosol plume surveillance application.

2. Spuler, S. M. and Mayor, S. D. Scanning eye-safe elastic backscatter lidar at 1.54 microns. *J. Atmos. Ocean. Technol.*, 22:696–703, 2005.
3. Mayor, S. D., Spuler, S. M., and Morley, B. M. Scanning eye-safe depolarization lidar at 1.54 microns and potential usefulness in bioaerosol plume detection. In *SPIE Conference on Laser Radar Technology and Applications IV*. SPIE, 2005.
4. Sassen, K. The polarization lidar technique for cloud research: a review and current assessment. *Bull. Amer. Meteor. Soc.*, 72:1848–1866, 1991.
5. Liou, K.-N. and Lahore, H. Laser sensing of cloud composition: a backscattered depolarization technique. *J. Appl. Meteor.*, 13:257–263, 1974.
6. Liou, K.-N. and Schotland, R. M. Multiple backscattering and depolarization from water clouds from a pulsed lidar system. *J. Atmos. Sci.*, 28:772–784, 1971.
7. Bissonnette, L. R., Roy, G., and Fabry, F. Range-height scans of lidar depolarization for characterizing properties and phase of clouds and precipitation. *J. Atmos. Ocean. Technol.*, 18:1429–1446, 2001.
8. Grubisic, V., Doyle, J. D., Kuettner, J., Poulos, G. S., and Whiteman, C. D. Terrain-induced rotor experiment (t-rex) scientific overview document and experiment design. Technical report, Available at <http://www.joss.ucar.edu/trex>, 2004.